1670 *Inorg. Chem.* **2011**, *50*, 1670–1681
DOI: 10.1021/ic102111t

Inorganic Chemistry
Article

# Synthesis, Structure Elucidation, and Redox Properties of $^{99}$Tc Complexes of Lacunary Wells−Dawson Polyoxometalates: Insights into Molecular $^{99}$Tc−Metal Oxide Interactions

**Donna McGregor,[†,‡,#] Benjamin P. Burton-Pye,[†,#] Robertha C. Howell,[†] Israel M. Mbomekalle,[†,⊥] Wayne W. Lukens Jr.,[§] Fang Bian,[†,‡] Edward Mausolf,[∥] Frederic Poineau,[∥] Kenneth R. Czerwinski,[∥] and Lynn C. Francesconi*[,†,‡]**

[†]*Hunter College of the City University of New York, 695 Park Avenue, New York, New York 10065, United States,* [‡]*Graduate Center of the City University of New York, New York, New York 10016, United States,* [§]*Chemical Sciences Division, The Glenn T. Seaborg Center, E.O. Lawrence Berkeley National Laboratory (LBNL), One Cyclotron Road, Berkeley, California 94720, United States, and* [∥]*Department of Chemistry, University of Nevada Las Vegas, Las Vegas, Nevada 89154, United States .* [⊥]*Present address: Institut Lavoisier, UMR8180, Université de Versailles St. Quentin, 45 Avenue des Etats-Unis, 78035 Versailles Cedex, France.* [#]*These authors contributed equally to this work.*

Received October 19, 2010

The isotope $^{99}$Tc ($\beta_{max}$, 293.7; half-life, $2.1 \times 10^5$ years) is an abundant product of uranium-235 fission in nuclear reactors and is present throughout the radioactive waste stored in underground tanks at the Hanford and Savannah River sites. Understanding and controlling the extensive redox chemistry of $^{99}$Tc is important in identifying tunable strategies to separate $^{99}$Tc from spent fuel and from waste tanks and, once separated, to identify and develop an appropriately stable waste form for $^{99}$Tc. Polyoxometalates (POMs), nanometer-sized models for metal oxide solid-state materials, are used in this study to provide a molecular level understanding of the speciation and redox chemistry of incorporated $^{99}$Tc. In this study, $^{99}$Tc complexes of the $(\alpha_2\text{-}P_2W_{17}O_{61})^{10-}$ and $(\alpha_1\text{-}P_2W_{17}O_{61})^{10-}$ isomers were prepared. Ethylene glycol was used as a "transfer ligand" to minimize the formation of $TcO_2 \cdot xH_2O$. The solution structures, formulations, and purity of $Tc^VO(\alpha_1/\alpha_2\text{-}P_2W_{17}O_{61})^{7-}$ were determined by multinuclear NMR. X-ray absorption spectroscopy of the complexes is in agreement with the formulation and structures determined from $^{31}$P and $^{183}$W NMR. Preliminary electrochemistry results are consistent with the EXAFS results, showing a facile reduction of the $Tc^VO(\alpha_1\text{-}P_2W_{17}O_{61})^{7-}$ species compared to the $Tc^VO(\alpha_2\text{-}P_2W_{17}O_{61})^{7-}$ analog. The $\alpha_1$ defect is unique in that a basic oxygen atom is positioned toward the $\alpha_1$ site, and the $Tc^VO$ center appears to form a dative metal−metal bond with a framework W site. These attributes may lead to the assistance of protonation events that facilitate reduction. Electrochemistry comparison shows that the $Re^V$ analogs are about 200 mV more difficult to reduce in accordance with periodic trends.

## Introduction

The isotope $^{99}$Tc ($\beta_{max}$, 293.7 keV; half-life, $2.1 \times 10^5$ years) is of interest and concern for two reasons: (1) $^{99}$Tc is a major product of uranium-235 fission in nuclear reactors (~6% thermal neutron fission yield) and (2) large amounts of $^{99}$Tc, formed during early plutonium production activities, are present in the radioactive waste stored in underground tanks at Hanford and Savannah River.[1,2]

The physical properties of $^{99}$Tc and its complex redox activity pose a problem for both closing the nuclear fuel cycle and remediation of waste tanks. In a storage repository, the long half-life of $^{99}$Tc means that its waste form must be resistant to degradation. Understanding and controlling the extensive redox chemistry of Tc is important in identifying strategies to separate it from the tank waste and spent nuclear fuel and is important in the identification and development of an appropriately stable waste form for $^{99}$Tc once separated from spent nuclear fuel and from waste tanks.

The interplay between the specific oxidation state of $^{99}$Tc and the "ligands" present in the tank waste or the coordination environment in a specific storage material determines the speciation and stability of the Tc within those materials. One crucial gap in the knowledge that needs to be filled to address both the separation from tank waste and design of storage matrices is a molecular level understanding of the factors that control the oxidation state of $^{99}$Tc in metal−oxide matrices.

*To whom correspondence should be addressed. E-mail: lfrances@hunter.cuny.edu.

(1) Beals, D. M.; Hayes, D. W. *Sci. Total Environ.* **1995**, *173*, 101.
(2) Hunt, A. G.; Skinner, T. E. *Hydrogeol. J.* **2010**, *18*, 381.

 Published on Web 01/26/2011 

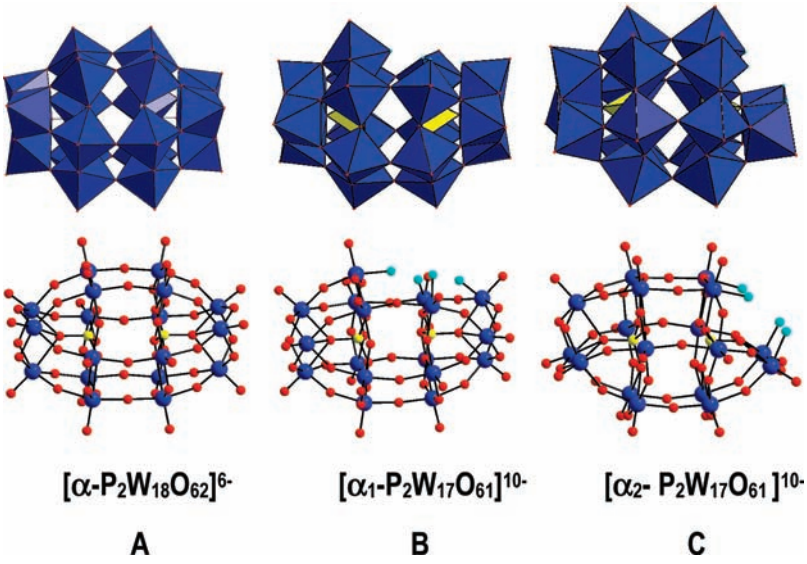


**Figure 1.** The plenary Wells−Dawson ion and lacunary Wells−Dawson isomers. Top: polyhedral representation. Bottom: ball and stick representation. (A) $(\alpha\text{-}P_2W_{18}O_{62})^{6-}$ is the "plenary" or parent Wells−Dawson ion, ca. 1.2 nm in length and 0.6 nm in width. (B) Removal of a "belt" W from the plenary Wells−Dawson structure gives the "lacunary" $(\alpha_1\text{-}P_2W_{17}O_{61})^{10-}$ isomer. (C) Removal of a "cap" W from the plenary Wells−Dawson gives the $(\alpha_2\text{-}P_2W_{17}O_{61})^{10-}$ isomer. The terminal oxygen atoms in the defects are shown in cyan. The defect structures possess distinct and different electronic and steric features that impact chemical and redox speciation of $^{99}$Tc.

In nuclear waste and in aerobic environments, the most stable Tc oxidation state is Tc(VII), which is highly environmentally mobile and generally not appropriate for disposal in a waste repository. In most existing and proposed waste forms, the desired oxidation state is Tc(IV) since Tc(IV) is not environmentally mobile. Also, the ionic radius of Tc(IV) is similar to that of Ti(IV) and Fe(III), which may allow Tc(IV) to be incorporated into the lattices of titanium or iron oxides.[3−6]

Polyoxometalates (POMs) are soluble nanometer-sized models for metal oxide solid-state materials.[7−9] We postulate that POMs, polyanionic aggregates of early transition metals ($Mo^{VI}$ and $W^{VI}$), may provide an understanding of the coordination chemistry, oxidation state, and speciation of $^{99}$Tc incorporated into metal oxides. The $MO_6$ octahedron is the principal building block of POMs; the transition metals are generally in their $d^0$ oxidation states held together by metal−oxygen bonds. The octahedra are condensed to form aggregates primarily by sharing oxygen atoms in a $\mu$-oxo linkage at corners and in a di-$\mu$-oxo linkage at edges of the polyhedra. Oxygen atoms of the "plenary" structures of POMs, such as the Wells−Dawson anion, $(\alpha\text{-}P_2W_{18}O_{62})^{6-}$ (Figure 1), are close packed, simulating solid oxide structures.[10] Polyoxometalates possess alternating bond order differences, resulting in rings exhibiting alternating short−long O−M−O bonds.[10] Binding of counterions and protonation dynamics of the POMs may be analogous to the dynamics found in solid-state metal oxide materials.

In this study, the $(\alpha_2\text{-}P_2W_{17}O_{61})^{10-}$ and $(\alpha_1\text{-}P_2W_{17}O_{61})^{10-}$ isomers that are derivatives of the "plenary" Wells−Dawson $(\alpha\text{-}P_2W_{18}O_{62})^{6-}$ POM, by removal of a $W{=}O^{3+}$ unit from the cap and belt regions, respectively, as shown in Figure 1, can be considered "defect" structures. These "lacunary" polyoxometalates serve as models for defect structures on a solid surface. The "mono-vacant" defect is comprised of four oxygen donor atoms that are available for bonding to technetium, Figure 1, and such oxide defects will bind "hard" Tc moieties.

The defects of POMs possess specific and distinct steric and electronic features that can affect coordination chemistry and impact the redox stability of technetium. Specifically, in this study, monovacant defect structures of the Wells−Dawson ion ($(\alpha_2\text{-}P_2W_{17}O_{61})^{10-}$ and $(\alpha_1\text{-}P_2W_{17}O_{61})^{10-}$ isomers) possess defects with clearly different steric and electronic properties, Figure 1. These $\alpha_1$ and $\alpha_2$ defects have different redox properties and binding strengths to transition metals. Studies on lanthanide and transition metal POM speciation support the notion that the high basicity of the $\alpha_1$ vacancy requires high charge/size cations for stabilization.[11−22] The elevated basicity of the $\alpha_1$ defect is ascribed by Contant and Ciabrini[13]

(3) Khalil, M. Y.; White, W. B. *J. Am. Ceram. Soc.* **1983**, *66*, C197.
(4) Langton, C. A. *Challenging Applications for Hydrated and Chemically Reacted Ceramics*; Savannah River Lab: Aiken, SC, **1988**.
(5) Langton, C. A. *Mater. Res. Soc. Symp. Proc.* **1988**, *112*, 61.
(6) Singh, D.; Mandalika, V. R.; Parulekar, S. J.; Wagh, A. S. *J. Nucl. Mater.* **2006**, *348*, 272.
(7) Fang, X.; Hill, C. L. *Angew. Chem., Int. Ed.* **2007**, *46*, 3877.
(8) Day, V. W.; Klemperer, W. G.; Schwartz, C.; Wang, R.-C. In *Surface Organometallic Chemistry: Molecular Approaches to Surface Catalysis*; Kluwer Academic Publishers: New York, 1988; p 173.
(9) Long, D.-L.; Burkholder, E.; Cronin, L. *Chem. Soc. Rev.* **2007**, *36*, 105.
(10) Day, V. W.; Klemperer, W. G. *Science* **1985**, *228*, 533.
(11) Abbessi, M.; Contant, R.; Thouvenot, R.; Herve, G. *Inorg. Chem.* **1991**, *30*, 1695.
(12) Boglio, C.; Lenoble, G.; Duhayon, C.; Hasenknopf, B.; Thouvenot, R.; Zhang, C.; Howell, R. C.; Burton-Pye, B. P.; Francesconi, L. C.; Lacote, E.; Thorimbert, S.; Malacria, M.; Afonso, C.; Tabet, J.-C. *Inorg. Chem.* **2006**, *45*, 1389.
(13) Ciabrini, J.-P.; Contant, R. *J. Chem. Research* **1993**, *391*, 2720.
(14) Contant, R.; Abbessi, M.; Canny, J.; Belhouari, A.; Keita, B.; Nadjo, L. *Inorg. Chem.* **1997**, *36*, 4961.
(15) Contant, R.; Ciabrini, J.-P. *J. Chem. Res.* **1982**, 641.
(16) Contant, R.; Richet, M.; Lu, Y. W.; Keita, B.; Nadjo, L. *Eur. J. Inorg. Chem.* **2002**, 2587.
(17) Harmalker, S. P.; Leparulo, M. A.; Pope, M. T. *J. Am. Chem. Soc.* **1983**, *105*, 4286.
(18) Keita, B.; Girard, F.; Nadjo, L.; Contant, R.; Canny, J.; Richet, M. *J. Electroanal. Chem.* **1999**, *478*, 76.
(19) Leparulo-Loftus, M. A.; Pope, M. T. *Inorg. Chem.* **1987**, *26*, 2112.

to the orientation of the $PO_4^{3-}$ tetrahedron within the cavity of the W−O framework, positioning a basic oxygen atom near the $\alpha_1$ site. Transition metal cations substituted into the $\alpha_1$ (belt) position are more readily reduced than when substituted in the $\alpha_2$ (cap) position.[14,16,18,23,24]

In this study, $^{99}$Tc complexes of the $(\alpha_2\text{-}P_2W_{17}O_{61})^{10-}$ and $(\alpha_1\text{-}P_2W_{17}O_{61})^{10-}$ isomers are prepared and characterized by multinuclear NMR and X-ray absorption spectroscopy, and preliminary electrochemical studies are reported. The reduction and oxidation of $Tc^V$ is compared in these isomeric complexes along with the reduction and oxidation of the $Re^V$ analogs. We attempt to identify the features of the polyoxometalate that impact reduction potentials of technetium.

**Key Prior Studies of Related Tc and Re POMs.** Rhenium, Re, the third row congener of Tc, has been used as a nonradioactive surrogate for Tc. Re possesses higher reduction potentials, slower kinetics, and often an expanded coordination sphere compared with Tc[25−27] and should be used with caution as a Tc substitute.

The $(Re^VO)^{3+}$ and $(Tc^VO)^{3+}$ units have been introduced into the lacunary α-Keggin, $\alpha\text{-}XW_{11}O_{39}^{n-}$ (X = P, $n$ = 7; X = Si, $n$ = 8).[28,29] The purity of these analogs has been demonstrated by IR, electrochemistry, mass spectrometry, and EPR ($Re^{VI}$). We have isolated pure $Re^{V,VI,VII}$ $(\alpha_2\text{-}P_2W_{17}O_{61})^{10-}$ complexes as verified by $^{31}$P and $^{183}$W NMR spectroscopy along with the above-mentioned techniques.[30] A slight modification of crystallization using acidic conditions of the aqueous $Re^VO\text{−}\alpha_2\text{-}P_2W_{17}O_{61}$ complex resulted in a 2:2 dimer.[31]

## Experimental Section

**General.** All materials were purchased as reagent grade and used without further purification. Potassium hexachlororhenate was purchased from Aldrich (99.99% purity). $^{99}$Tc is a weak $\beta$-emitter with a half-life of $2 \times 10^5$ years. All syntheses and sample preparations were performed in laboratories approved for low-level use of radioactivity using appropriate radioactive material handling procedures. $^{99}TcO_4^-$ was purchased as the ammonium salt from Oak Ridge National Laboratory and treated with $H_2O_2$ to oxidize any reduced Tc.[32] $(NBu_4)TcOCl_4$ was prepared from $NH_4TcO_4$ according to an established procedure.[33] $K_9Li(\alpha_1\text{-}P_2W_{17}O_{61})$ (α1) and $K_{10}(\alpha_2\text{-}P_2W_{17}O_{61})$ (α2) ligands were prepared as described in the literature.[13,34] The preparation of $\alpha_1\text{-}[Fe(H_2O)P_2W_{17}O_{61}]^{7-}$ (Fe-α1) and $K_{7-n}H_n[Re^VO(\alpha_2\text{-}P_2W_{17}O_{61})]$ ($Re^VO$-α2) for electrochemistry was described previously.[30,34] Analytical grade $CH_3COONa$ (Fisher) and glacial $CH_3COOH$ (Acros) were used as received. Centrifugations were performed with an International Equipment Co. Model CL Clinical centrifuge. Pure water used throughout was obtained using a Millipore Direct Q5 system (conductivity = 18 μΩ). Infrared analyses were performed on a Perkin-Elmer 1625 FTIR spectrometer. Negative-ion electrospray mass spectra were recorded on a VG Quattro at the University of Illinois School of Chemical Sciences Mass Spectrometry Resource.

**Collection of NMR Data.** NMR data were collected on a JEOL GX-400 spectrometer with 5 or 10 mm tubes fitted with a Teflon insert that were purchased from Wilmad Glass. Resonance frequencies are 161.8 MHz for $^{31}$P and 16.7 for $^{183}$W. Chemical shifts are given with respect to external 85% $H_3PO_4$ for $^{31}$P and 2.0 M $Na_2WO_4$ for $^{183}$W. Typical acquisition parameters for $^{31}$P spectra included the following: spectral width, 10 000 Hz; acquisition time, 0.8 s; pulse delay, 1 s; pulse width, 15 μs (50° tip angle). From 200 to 1000 scans were required. For $^{183}$W spectra, typical conditions included the following: spectral width, 10 000 Hz; acquisition time, 1.6 s; pulse delay, 0.5 s; pulse width, 50 μs (45° tip angle). From 1000 to 30 000 scans were acquired. For all spectra, the temperature was controlled to ±0.2°. For the $^{31}$P and $^{183}$W chemical shifts, the convention used is that the more negative chemical shifts denote more upfield resonances.

**Extended X-Ray Absorption Fine Structure (EXAFS) Spectroscopy.** Samples were dissolved in 1 mL of 18 MΩ water then transferred to 2 mL screw-capped, polypropylene centrifuge tubes, which where sealed inside two nested polyethylene bags. Using these samples, data were acquired at room temperature in transmission mode Ar-filled ion chambers at SSRL beamlines 11−2 and 4−1; data were collected using the locally written program XAScollect. The harmonic content of the beam was reduced by detuning the monochromator by 50%. The data were processed using EXAFSPAK and Athena/ifeffit.[35,36] Data were fit using Artemis/ifeffit and theoretical phases and amplitudes calculated using FEFF7.[37] The initial model used in the FEFF calculation was $(NH_4)_6(P_2W_{18}O_{62})$ with one W atom replaced by Tc.[38] Additional scattering shells were added only if their inclusion lowered the value of reduced $\chi$-squared.

The F-test was used to analyze the significance of the fitting parameters including the significance of adding a scattering shell.[39] The null hypothesis is that the additional shell of atoms does not improve the fit. The result of the F-test is the probability, $p$, that this hypothesis is correct. If $p < 0.05$, the null hypothesis is rejected in favor of the alternative hypothesis that the additional shell significantly improves the fit.[40]

**Electrochemical Data Collection.** Electrochemical data were obtained using a BAS Voltammetric Analyzer System controlled by the BAS CV-50W software (for PC). The cell used for cyclic voltammetry (CV) contained a glassy-carbon working electrode (BAS standard disk electrode, 3 mm OD), a Pt wire auxiliary electrode (0.5 mm), and a BAS Ag/AgCl (3 M NaCl) reference electrode.

The electrochemistry of the compounds was conducted at a concentration of 0.2 mM in a pH 5 buffer (0.5 M $NaSO_4$ in 0.01 M NaOAc). Prior to obtaining electrochemical data, solutions were

(20) Sadakane, M.; Dickman, M. H.; Pope, M. T. *Inorg. Chem.* **2001**, *40*, 2715.
(21) Sadakane, M.; Ostuni, A.; Pope, M. T. *J. Chem. Soc., Dalton Trans.* **2002**, 63.
(22) Zhang, C.; Howell, R. C.; Luo, Q.; Fieselmann, H. L.; Todaro, L.; Francesconi, L. C. *Inorg. Chem.* **2005**, *44*, 3569.
(23) Contant, R.; Herve, G. *Rev. Inorg. Chem.* **2002**, *22*, 63.
(24) Contant, R.; Thouvenot, R. *Inorg. Chim. Acta* **1993**, *212*, 41.
(25) *The Inorganic Chemistry of Technetium and Rhenium As Relevant to Nuclear Medicine*; Deutsch, E., Libson, K., Vanderheyden, J.-L., Eds.; Cortina International: Verona, Italy, 1990; Vol. *3*.
(26) Libson, K.; Woods, M.; Sullivan, J.; Watkins, J. W., II; Elder, R. C.; Deutsch, E. *Inorg. Chem.* **1988**, *27*, 999.
(27) VanderHeyden, J.-L.; Heeg, M. J.; Deutsch, E. A. *Inorg. Chem.* **1985**, *24*, 1666.
(28) Abrams, M. J.; Costello, C. E.; Shaikh, S. N.; Zubieta, J. *Inorg. Chim. Acta* **1991**, *180*, 9.
(29) Ortega, F.; Pope, M. T. *Inorg. Chem.* **1984**, *23*, 3292.
(30) Venturelli, A.; Nilges, M. J.; Smirnov, A.; Belford, R. L.; Francesconi, L. C. *J. Chem. Soc., Dalton Trans.* **1999**, 301.
(31) Kato, C. N.; Hara, K.; Hatano, A.; Gogo, K.; Kuribayashi, T.; Hayashi, K.; Shinohara, A.; Kataoka, Y.; Mori, W.; Nomiya, K. *Eur. J. Inorg. Chem.* **2008**, *2008*, 3134.
(32) Boyd, G. E. *J. Chem. Educ.* **1959**, *36*, 3.
(33) Davison, A.; Trop, H.; DePamphilis, B.; Jones, A. *Inorg. Synth.* **1982**, *21*, 160.
(34) Contant, R. *Inorg. Synth.* **1990**, *27*, 71.
(35) Newville, M. J. *Synchrotron Radiat.* **2001**, *8*, 322.
(36) Ravel, B. *Phys. Scr.* **2005**, *T115*, 1007.
(37) Rehr, J. J.; Albers, R. C.; Zabinsky, S. I. *Phys. Rev. Lett.* **1992**, *69*, 3397.
(38) D'Amour, V. H. *Acta Crystallogr.* **1976**, *B32*, 729.
(39) Bevington, P. R.; Robinson, K. D. *Data Reduction and Error Analysis for the Physical Sciences*; McGraw-Hill: Boston, MA, 1992.
(40) Downward, L.; Booth, C. H.; Lukens, W. W.; Bridges, F. In *AIP Conference Proceedings 2007*; American Institute of Physics: College Park, MD, 2007; Vol. *882*, p 129.

**Table 1.** Multinuclear NMR Data for $Tc^{V}-\alpha_1/\alpha_2-P_2W_{17}O_{61}$ Complexes[a]

| compound | solvent | $^{31}$P NMR, $\delta$ (ppm) | $^{183}$W NMR, $\delta$ (ppm) |
|---|---|---|---|
| $Tc^{V}O$-α2 | $D_2O$ | −11.60 (1), −13.16 (1) | −131.06 (2), −161.51 (1), −179.91 (2), −181.72 (2), −192.19 (2), −195.23 (2), −199.69 (2), −214.82 (2), −228.78 (2) |
| $Tc^{V}O$-α1 | $D_2O$ | −11.60 (1), −12.72 (1) | 37.21 (1), −117.85 (1), −120.78 (1), −132.83 (1), −147.71 (1), −172.40 (1), −173.08 (1), −174.01 (1), −185.67 (1), −188.84 (1), −189.09 (1), −190.01 (2), −203.29 (1), −204.70 (2), −229.39 (1) |
| $Re^{V}O$-α1 | $D_2O$ | −12.02 (1), −12.33 (1) | 35.17(1), −108.55(1), −111.43(1), −157.35(1), −167.90(1), −180.02(2), −184.51(1), −197.41(1), −208.1 (2), −228.77(1), −237.95(1), −242.69(1), −258.18(1), −308.79(1), −398.52(1). |

[a] See text for conditions. All spectra were taken at room temperature, 25 °C.

deaerated for at least 30 min with high purity Ar. A positive pressure of this gas was maintained during subsequent work. Preparation, including fine polishing of the glassy-carbon working electrode, was adapted from the procedure of Keita and coworkers.[41] Unless indicated otherwise, scan rates were 10 mV $s^{-1}$, and all experiments were carried out at ambient temperature under an atmosphere of Ar.

**Synthesis of Compounds. $K_{7-n}H_n[Tc^{V}O(\alpha_1\text{-}P_2W_{17}O_{61})]$ ($Tc^{V}O$-α1).** To a 20 mL scintillation vial containing a yellow/green solution of $(NBu_4)$ $TcOCl_4$ (100 mg, 0.2 mmol) dissolved in 1 mL of MeOH was added 60 $\mu$L (0.98 mmol) of ethylene glycol $(CH_2OH)_2$ (eg) to produce a blue/green $TcO(eg)_2^-$ complex. This solution was quickly added to a clear, colorless solution of α1 (447 mg, 0.099 mmol) dissolved in 5 mL of $H_2O$ containing LiCl (10 mg, 0.2 mmol). The resulting dark red solution and brown suspension was stirred for 3 min. The reaction mixture was centrifuged (15 min, 70 000 rpm) and the red supernatant decanted. KCl (0.16 g, 2 mmol) was added to the supernatant and was stored at room temperature for up to 48 h to allow any unreacted α1 (as monitored by $^{31}$P NMR) to precipitate. The mixture exhibiting a clean, two peak $^{31}$P NMR was filtered and 20 mL of ethanol added to the filtrate to precipitate a dark red solid, which was collected by vacuum filtration.

Yield: 40−60% based on $(NBu_4)TcOCl_4$. IR (KBr, $cm^{-1}$): 790 $cm^{-1}$ (strong, broad), 953 $cm^{-1}$ (weak), 1086 $cm^{-1}$ (strong).

**$K_{7-n}H_n[Tc^{V}O(\alpha_2\text{-}P_2W_{17}O_{61})]$ ($Tc^{V}O$-α2).** To a 20 mL scintillation vial containing a yellow/green solution of $(NBu_4)TcOCl_4$ (100 mg, 0.2 mmol) dissolved in 1 mL of MeOH was added 60 $\mu$L (0.98 mmol) of ethylene glycol to produce a blue/green $TcO(eg)_2^-$ complex. This solution was added quickly to a clear, colorless solution of α2 (447 mg, 0.099 mmol) dissolved in 5 mL of $H_2O$ at 80 °C. The resulting dark red solution and brown suspension was stirred for 3 min. While still warm, the reaction mixture was centrifuged (15 min, 70 000 rpm), the dark red supernatant decanted, and KCl (0.16 g, 2 mmol) added. The red solution was allowed to sit at room temperature for up to 72 h to allow any unreacted α2 (as monitored by $^{31}$P NMR) to precipitate. The mixture exhibiting a clean, two peak $^{31}$P NMR spectrum of the product was filtered, and 10 mL of ethanol was added to the filtrate to precipitate a dark red solid, which was collected by vacuum filtration.

Yield: 40−60% based on $(NBu_4)TcOCl_4$. IR (KBr, $cm^{-1}$): 790 $cm^{-1}$ (strong, broad), 953 $cm^{-1}$ (weak), 1086 $cm^{-1}$ (strong).

**$K_{7-n}H_n[Re^{V}O(\alpha_1\text{-}P_2W_{17}O_{61})]$ ($Re^{V}O$-α1).** A 200 mL round-bottom flask was charged with $K_2ReCl_6$ (0.285 g, 0.6 mmol) and α1 (2.39 g, 0.48 mmol), and deoxygenated water was added (30 mL) to form a slurry. The slurry was heated at 40 °C for 30 min, producing a navy blue solution. The solution was cooled to room temperature, 125 mL of ethanol added, and the sample placed in the freezer for 10 min. The dark microcrystalline solid was isolated by filtration and recrystallized twice from 50 mL of hot water. The product was 95% pure as judged by $^{31}$P NMR. Yield: 1.08 g, 0.22 mmol. In order to remove impurities arising from the $Re^{V}O$-α2 congener, 0.4 g of recrystallized product was dissolved in 5 mL of distilled water and loaded onto a silica column (5.5 cm (diameter) × 60 cm filled to a height of 40 cm with silica) primed with methanol and eluted with methanol. The dark blue fraction containing $Re^{V}O$-α1 was reduced in volume by rotary evaporation and filtered to remove any silica. The solvent was then removed by rotary evaporation to yield pure $Re^{V}O$-α1, free from $Re^{V}O$-α2.

The $^{31}$P NMR and $^{183}$W NMR data for the complexes are given in Table 1.

## Results and Discussion

**Synthesis of Complexes.** The synthesis of pure transition metal polyoxometalates is often complicated by the difficulty in separating unreacted POM ligands from the metal POM complex. Usually, separations are achieved by fractional crystallizations and are complicated by the similar solubilities of the metal complexes of POMs and the POM ligands. Separations are rendered even more difficult due to the small volumes manipulated in fractional crystallizations when working with milligram quantities of $^{99}$Tc. The small volumes, multiple oxidation states accessible to $^{99}$Tc, and hydrolysis of the $^{99}TcOCl_4^-$ starting reagent generally compromise the separation of the reactant from the products, reproducibility, and yield of the reactions

The $(NBu_4)TcOCl_4$ starting reagent readily hydrolyzes in water and in methanol; in order to stabilize this source of $Tc^{V}O$, $(NBu_4)TcOCl_4$ was treated with ethylene glycol, which acts as a "transfer ligand"[42] to inhibit the hydrolysis of $TcOCl_4^-$, stabilize the $Tc^{V}O$ core, and facilitate transfer of the $Tc^{V}O$ moiety for isolation of $Tc^{V}O$-α1 and $Tc^{V}O$-α2. The $TcO(eg)_2^-$ complex[43] was formed *in situ*, and the ethylene glycol ligands were replaced by the tetradentate α1/α2 ligands to form the $Tc^{V}$ complexes. The transfer ligand protocol used here is similar to those used in radiopharmaceutical kits (that employ the clinical isotope $^{99m}$Tc on the tracer level) where ligands such as glucoheptonate form weak complexes to stabilize the $^{99m}Tc^{V}O$ core for eventual substitution into the desired $^{99m}Tc^{V}O$ radiopharmaceutical.

(41) Keita, B.; Girard, F.; Nadjo, L.; Contant, R.; Belghiche, R.; Abessi, M. *J. Electroanal. Chem.* **2001**, *508*, 70.

(42) DePamphilis, B. V.; Jones, A. G.; Davison, A. *Inorg. Chem.* **1983**, *22*, 2292.

(43) Davison, A.; DePamphilis, B. V.; Jones, A. G.; Franklin, K. L.; Lock, C. J. L. *Inorg. Chim. Acta* **1987**, *128*, 161.

We found that a 1:1 Tc/α1 and α2 stoichiometry and a Tc/eg ratio of between 1:3.5 and 1:6 were required to obtain an optimal yield and purity. A ratio of less than 1:3.5 resulted in the formation of an increased amount of both a dark solid, presumed to be mostly $TcO_2 \cdot H_2O$, and free α1 or α2 ligand. A ratio of more than 1:6 resulted in a low yield and increased difficulty when isolating a pure product as a solid. The synthetic conditions balance the hydrolysis of the $TcOCl_4^-$ starting material to $TcO_2 \cdot H_2O$ and incorporation of Tc(V)O into the α1 and α2 frameworks. The development of the synthesis, inhibition of $TcO_2 \cdot H_2O$ formation, and formation of a $Tc^{IV}-(\mu\text{-}O)_2\text{-}Tc^{IV}$ α1/α2 dimer, or a $Tc^{IV}\text{-}(\mu\text{-}O)_2\text{-}Tc^{IV}$ ethyleneglycol complex, as found from EXAFS and XANES, will be discussed in a separate publication.

$Re^{V}O$-α1 was initially prepared in the same fashion as reported for $Re^{V}O$-α2; however, the preparation resulted in the formation of the parent Wells−Dawson ion, $(\alpha\text{-}P_2W_{18}O_{62})^{6-}$, and $Re^{V}O$-α2 impurities. Elevated temperatures increased the amount of $P_2W_{18}O_{62}^{6-}$ and $Re^{V}O$-α2. Running the reaction at lower temperatures reduced the amount of $P_2W_{18}$ and $Re^{V}O$-α2 but did not eliminate the formation of these impurities entirely. Multiple recrystallizations were attempted to isolate pure $Re^{V}O$-α1, but trace amounts of the $Re^{V}O$-α2 isomer were visible by $^{31}P$ NMR. Column chromatography utilizing silica gel as the stationary phase and employing methanol as an eluent separated the $Re^{V}O$-α2 from $Re^{V}O$-α1. Figure S1 (Supporting Information) illustrates the purification process as monitored by $^{31}P$ NMR and cyclic voltammetry.

**Characterization of Complexes. Infrared Spectroscopy.** The infrared spectra of $Tc^{V}O$-α1 and $Tc^{V}O$-α2 show characteristic stretches at 790 $cm^{-1}$ (strong, broad), 907 $cm^{-1}$, 953 $cm^{-1}$ (weak), and 1086 $cm^{-1}$(strong). Representative IR spectra (KBr pellet) are shown in the Supporting Information, Figure S2. The IR spectra are, not surprisingly, similar to the parent $(P_2W_{18}O_{62})^{6-}$. In a study by Ortega and Pope, the IR spectra for $Re^{V}$, $Re^{VI}$, and $Re^{VII}$ substituted into the $XW_{11}O_{39}^{n-}$ framework are similar to the parent $XW_{12}O_{40}^{(n+2)-}$.[29] We observed also that the IR spectra for $Re^{V}$, $Re^{VI}$, and $Re^{VII}$ substituted into the $(\alpha_2\text{-}P_2W_{17}O_{61})^{10-}$ framework are similar to that of the parent $(P_2W_{18}O_{62})^{6-}$.[30] The Tc=O stretch is expected to occur at 900−960 $cm^{-1}$, and that would overlap with the bands observed in the W framework.

**Mass Spectrometry.** Negative-ion electrospray mass spectrometry provides data with minimal fragmentation and has been found to be a useful tool for the analysis of polyoxometalates.[12,30,44,45] The data for the mass spectrometry analysis of $Tc^{V}O$-α1 and $Tc^{V}O$-α2 are presented in Table 2. The highly negatively charged molecules form adducts with cations, and thus different charge states can be formed. In aqueous solution, the −4, −3, and −2 charge state clusters are observed. Table 2 and Figure S3 (Supporting Information) show the corresponding $m/z$ values for the various charge states of the molecules with variable amounts of potassium and proton adducts. Taken with the multinuclear NMR data, *vide infra*, these mass spectral data confirm the formulation of the technetium complexes.

**Table 2.** Mass Spectrometry of the $Tc^{V}-\alpha_1/\alpha_2\text{-}P_2W_{17}O_{61}$ Complexes

| compound | ion | $m/z$ |
|---|---|---|
| $Tc^{V}O$-α2 | $K_4HTcO[P_2W_{17}O_{61}]^{2-}$ | 2217.9 |
| | $K_4TcO[P_2W_{17}O_{61}]^{3-}$ | 1478.5 |
| | $K_3HTcO[P_2W_{17}O_{61}]^{3-}$ | 1465 |
| | $K_2H_2TcO[P_2W_{17}O_{61}]^{3-}$ | 1453 |
| | $KH_3TcO[P_2W_{17}O_{61}]^{3-}$ | 1440 |
| | $H_4TcO[P_2W_{17}O_{61}]^{3-}$ | 1427 |
| | $K_2HTcO[P_2W_{17}O_{61}]^{4-}$ | 1089.6 |
| | $KH_2TcO[P_2W_{17}O_{61}]^{4-}$ | 1080.2 |
| | $H_3TcO[P_2W_{17}O_{61}]^{4-}$ | 1070.7 |
| $Tc^{V}O$-α1 | $K_4HTcO[P_2W_{17}O_{61}]^{2-}$ | 2217.8 |
| | $K_4TcO[P_2W_{17}O_{61}]^{3-}$ | 1477.6 |
| | $K_3HTcO[P_2W_{17}O_{61}]^{3-}$ | 1465 |
| | $K_3TcO[P_2W_{17}O_{61}]^{4-}$ | 1099 |
| | $K_2HTcO[P_2W_{17}O_{61}]^{4-}$ | 1089.8 |
| | $KH_2TcO[P_2W_{17}O_{61}]^{4-}$ | 1079.1 |
| | $H_3TcO[P_2W_{17}O_{61}]^{4-}$ | 1070.3 |

**Multinuclear NMR Spectroscopy.** Multinuclear NMR spectroscopy, given in Table 1, is used to establish the purity and structure of $Tc^{V}O$-α1, $Tc^{V}O$-α2, and $Re^{V}O$-α1. $^{31}P$ NMR is a well-established technique to assess impurities of polyoxometalates at the 2% level[46−48] and has been used to identify pure Wells−Dawson complexes of transition metals[46−50] and lanthanides.[12,20−22,49,51−56] (We also turn to electrochemistry to clearly observe signature patterns that identify the α1 and α2 isomer ligands[18,57] and to corroborate $Tc^{V}$ and $Re^{V}$ substitution into the $\alpha_1$ and $\alpha_2$ frameworks, *vide infra*.) The $^{31}P$ NMR spectra along with the $^{183}W$ spectra are presented in Figure 2 and Figure S4 (Supporting Information) for $Tc^{V}O$-α1 and $Tc^{V}O$-α2. The $^{31}P$ NMR spectra establish that the purities of the $Tc^{V}$ complexes of α1 and α2 are greater than 98%. Two resonances are observed for the $Tc^{V}O$-α1 and $Tc^{V}O$-α2 species. The upfield resonance is assigned to P1, the phosphorus atom close to the $Tc^{V}$ center, and the remote phosphorus, P2, is assigned to the downfield resonance.

$^{183}W$ NMR is used for structural identification of the $Tc^{V}$ complexes in solution. Each magnetically inequivalent tungsten atom presents one resonance, with P coupling and W−O−W coupling if the concentration, and thus intensity and resolution, is high enough. The $Tc^{V}O$-α2

(44) Bonchio, M.; Bortolini, O.; Conte, V.; Sartorel, A. *Eur. Jour. Inorg. Chem.* **2003**, *4*, 699.
(45) Deery, M. J.; Howarth, O. W.; Jennings, K. R. *J. Chem. Soc., Dalton Trans.* **1997**, 4783.
(46) Finke, R. G.; Droege, M. W.; Domaille, P. J. *Inorg. Chem.* **1987**, *26*, 3886.
(47) Finke, R. G.; Lyon, D. K.; Nomiya, K.; Sur, S.; Mizuno, N. *Inorg. Chem.* **1990**, *29*, 1784.
(48) Finke, R. G.; Rapko, B.; Saxton, R. J.; Domaille, P. J. *J. Am. Chem. Soc.* **1986**, *108*, 2947.
(49) Bartis, J.; Kunina, Y.; Blumenstein, M.; Francesconi, L. C. *Inorg. Chem.* **1996**, *35*, 1497.
(50) Jorris, T. L.; Kozik, M.; Casan-Pastor, N.; Domaille, P. J.; Finke, R. G.; Miller, W. K.; Baker, L. C. W. *J. Am. Chem. Soc.* **1987**, *109*, 7402.
(51) Bartis, J.; Dankova, M.; Lessmann, J. J.; Luo, Q.-H.; Horrocks, W. D., Jr.; Francesconi, L. C. *Inorg. Chem.* **1999**, *38*, 1042.
(52) Bartis, J.; Sukal, s.; Dankova, M.; Kraft, E.; Kronzon, R.; Blumenstein, M.; Francesconi, L. C. *J. Chem. Soc., Dalton Trans.* **1997**, 1937.
(53) Howell, R. C.; Perez, F. G.; Jain, S.; Horrocks, W. D., Jr.; Rheingold, A. L.; Francesconi, L. C. *Angew. Chem., Int. Ed.* **2001**, *40*, 4301.
(54) Salmonte, J. L.; Pope, M. T. *Can. J. Chem.* **2001**, *79*, 802.
(55) Zhang, C.; Bensaid, L.; McGregor, D.; Fang, X.; Howell, R. C.; Burton-Pye, B.; Q., L.; Todaro, L.; Francesconi, L. C. *J. Cluster Sci.* **2006**, *17*, 389.
(56) Zhang, C.; Howell, R. C.; Scotland, K. B.; Perez, F. G.; Todaro, L.; Francesconi, L. C. *Inorg. Chem.* **2004**, *43*, 7691.
(57) Keita, B.; Mbomekalle, I.-M.; Nadjo, L.; Contant, R. *Eur. J. Inorg. Chem.* **2002**, 473.

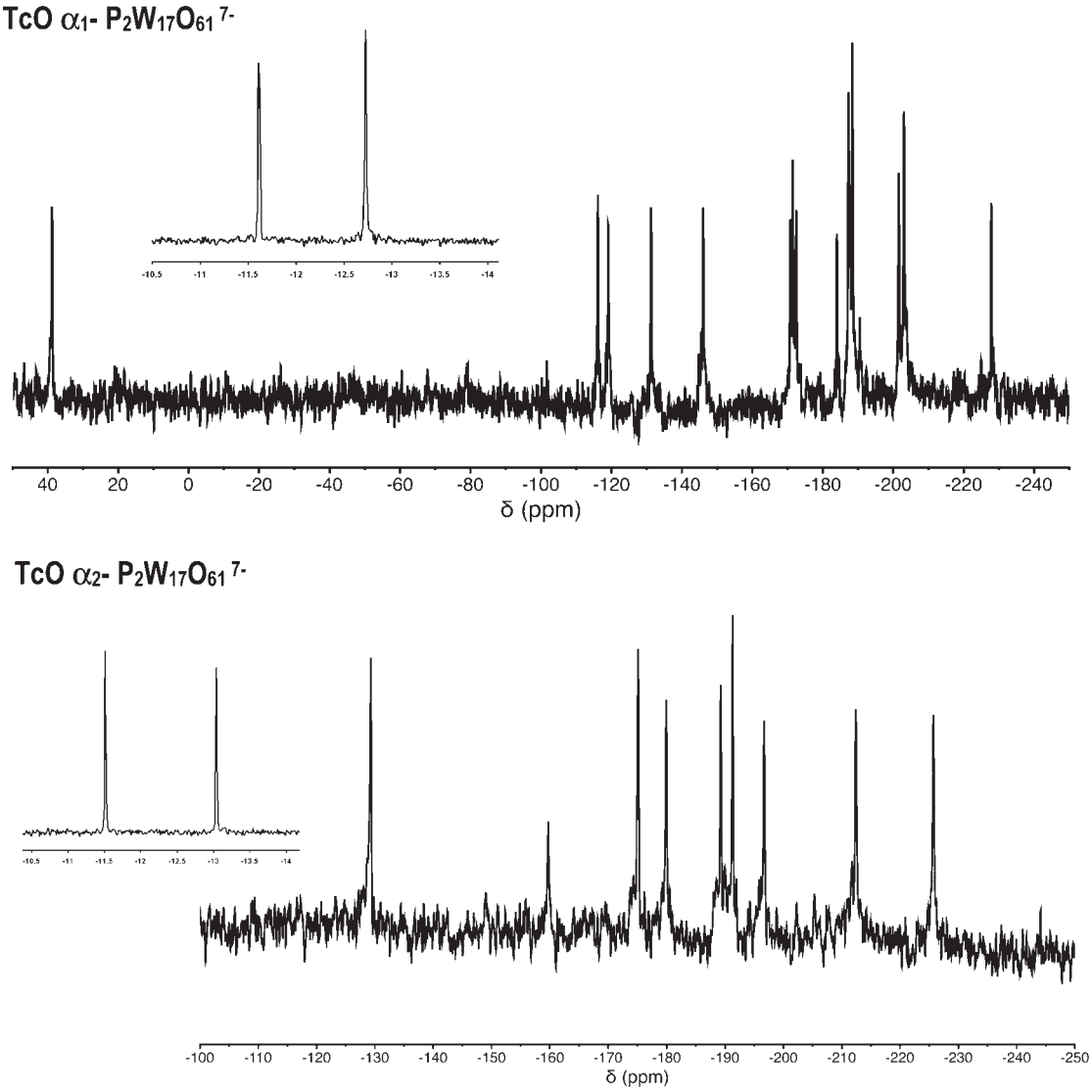


**Figure 2.** Multinuclear NMR Data for $Tc^{V}O$-α1 and $Tc^{V}O$-α2 taken at 25 °C in $D_2O$. Top: $^{31}P$ NMR data; bottom: $^{183}W$ NMR data.

clearly shows nine well-resolved resonances with appropriate integrations for incorporation of the $Tc^{V}O$ center into the cap region of the α2 lacunary polyoxometalate (Figure 2). This spectrum is different from free α2.[49,58] Incorporation of the $Tc^{V}O$ center into α1 is clearly identified by the $^{183}W$ NMR spectrum (Figure 2) as well. In this case, α1 possesses $C_1$ symmetry, and 17 resonances are observed in the $^{183}W$ NMR spectrum of the $Tc^{V}$ complex. The pattern observed in Figure 2 is clearly different from the $Tc^{V}O$-α2 species and from α1 and α2.[49,50] Although the resonances have not been assigned to specific tungsten atoms, the downfield resonance is likely attributed to a W atom close to the vacancy, *vide infra*. The cause of the downfield shift is discussed in detail in the EXAFS section of this manuscript. In summary, the mass spectroscopy confirms the expected formulations, and the multinuclear ($^{31}P$ and $^{183}W$) NMR spectroscopy is consistent with the $Tc^{V}O$ centers incorporating into the cap and belt regions of α2 and α1 ligands, respectively. The isolated, pure species were carried forward for comparison in electrochemical and X-ray absorption spectroscopy experiments, *vide infra*.

**X-Ray Absorption Fine Structure.** The X-ray absorption near edge structure (XANES) spectra of $TcO_4^-$, $TcO_2 \cdot 2H_2O$, $Tc^{V}O$-α1, and $Tc^{V}O$-α2 are shown in Figure 3. In this case, the energy of the absorption edge is a reflection of the amount of screening experienced by the 1s electrons. For this reason, the absorption edges of complexes with higher oxidation states typically occur at higher energies than those of complexes with lower oxidation states. This trend can, however, be complicated by the effects of covalency, which can shift the energy of the absorption edge from what would be expected on the basis of formal oxidation state alone. In the case of the complexes shown in Figure 3, the effects of covalency are anticipated to be minor compared with the effects of oxidation state. The half-height of the edges of $TcO_2 \cdot 2H_2O$, $Tc^{V}O$-α1, and $Tc^{V}O$-α2 with respect to that of $TcO_4^-$ are −6.7 eV, −3.2 eV, and −3.7 eV, respectively. The relative position of the Tc K-edge absorption edges of $Tc^{V}O$-α1 and $Tc^{V}O$-α2 with respect to $TcO_2 \cdot 2H_2O$ are consistent with the presence of Tc(V). In addition, the Tc center in $Tc^{V}O$-α2 is slightly more electron rich than that of $Tc^{V}O$-α1.

(58) Acerete, R.; Hammer, C. F.; Baker, L. C. W. *J. Am. Chem. Soc.* **1982**, *104*, 5384.

The XANES spectra also contain information about the symmetry of the coordination environment in $Tc^{V}O$-α1 and $Tc^{V}O$-α2. The small, well-defined peaks below 21050 eV are pre-edge features due to the 1s−4d transition, which is symmetry forbidden in centrosymmetric complexes. The presence of this feature in the spectra of $Tc^{V}O$-α1 and $Tc^{V}O$-α2 is consistent with the postulated, noncentrosymmetric structure.

Extended X-ray absorption fine structure (EXAFS) spectra can be used to determine the local structure of a particular chemical element. The Tc K-edge solution EXAFS of $Tc^{V}O$-α1 and $Tc^{V}O$-α2 are shown Figure 4 along with the EXAFS spectra of model complexes derived by fitting the data. To determine the local structure of the Tc sites, model complexes were created by replacing a tungsten atom in the cap ($Tc^{V}O$-α2) or the belt ($Tc^{V}O$-α1) of the Wells−Dawson plenary ion by a Tc center. The data were fit using shells of scattering atoms at increasing distances from the Tc center. If the value of reduced χ-squared decreased, the scattering shells were retained. The numbers of heavy atom (W, P) neighbors and nearest O neighbors were determined from the model, but the number of more distant oxygen neighbors were determined by varying this number to obtain the best fit.

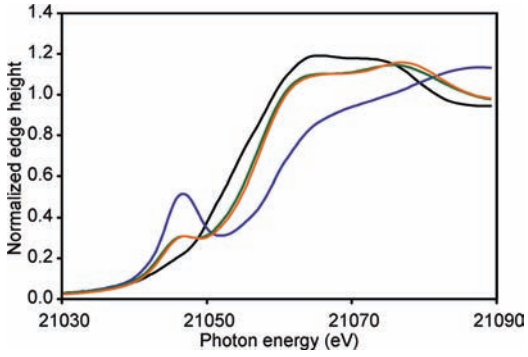


**Figure 3.** Tc K-edge XANES spectra of, from lowest energy to highest energy: $TcO_2 \cdot 2H_2O$ (black), $Tc^{V}O$-α2 (green), $Tc^{V}O$-α1 (orange), and $TcO_4^-$ (blue). Data obtained using SSRL beamline 4−1.

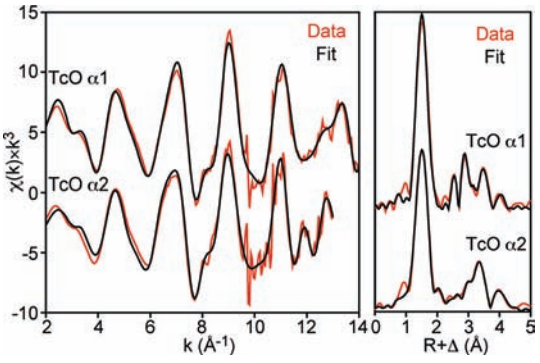


**Figure 4.** Tc K-edge EXAFS spectra (left) and Fourier transforms (right) for $Tc^{V}O$-α1 (upper) $Tc^{V}O$-α2 (lower). Data are shown in color, and fits are given in black. Data obtained using SSRL beamline 4−1.

**$Tc^{V}O$-α2.** The local structure obtained by fitting the EXAFS spectrum of $Tc^{V}O$-α2 complexes is consistent with the structure of the cap W site of the Wells−Dawson ion. The distances from the Tc atom to the neighboring atoms are given in Table 3.[59] In this case, $p(F)$ values for all scattering atoms are less than 0.05, so all atoms can be considered to be observed in the EXAFS experiment. The structure is consistent with a square pyramidal Tc(V). The oxygen coordination environment contains a very short Tc−O bond, 1.64 Å, which is consistent with the terminal oxo ligand of a Tc(V) ion, and the best fit is obtained with four oxygen ligands at 2.00 Å and a more distant oxygen neighbor at 2.53 Å. Scattering from more distant atoms, particularly P and W, is consistent with coordination of the Tc(V) ion by $(\alpha_2\text{-}P_2W_{17}O_{61})^{10-}$. The best fit is obtained with two neighboring W atoms at 3.43 Å, one neighboring P atom at 3.54 Å, and two more neighboring W atoms at 3.57 Å, in good agreement with the distances predicted if a W atom in the cap of the Wells−Dawson ion is replaced by a Tc atom. The major difference is that the terminal oxo of Tc(V) is much shorter than the terminal oxo of W(VI).

EXAFS data collected at the Advanced Photon Source, Argonne National Laboratory (Figure S5, Table S1, Supporting Information), on the $Tc^{V}O$-α2 are in excellent agreement with the above results. The Tc atom is 6-coordinate with oxygen atoms at 1.63(1) Å ($Tc^{V}O$), 1.93(2) Å, and 2.36(2) Å. The results from the APS further show W atoms at 3.43(3) Å and 3.57 (3) Å, a P atom at 3.48(3) Å, and an O atom at 3.98(4) Å, which is consistent with Tc(V) coordinated to $(\alpha_2\text{-}P_2W_{17}O_{61})^{10-}$.

**$Tc^{V}O$-α1.** Surprisingly, the local structure obtained by fitting the EXAFS spectrum of $Tc^{V}O$-α1 is not consistent with simply replacing a W atom in the belt of the Wells−Dawson ion by a Tc atom, as shown by the comparison of the bond distances derived by fitting the EXAFS spectrum with the local structure of the belt W atoms of the Wells−Dawson ion given in Table 4. Initial refinements using this model suggested that Tc possessed a neighboring atom at ∼3 Å. Furthermore, fitting of the nearest oxygen

**Table 3.** Best Fit Parameters for the EXAFS Spectrum for $K^+$ Salt of $Tc^{V}O$-$\alpha_2$[a]

| neighbor | # of neighbors[b] | distance (Å) | $\sigma^2$ (Å$^2$) | $p(F)$[b] | local structure of the "cap" tungsten site (Å)[c] |
|---|---|---|---|---|---|
| O | 1 | 1.638(4) | 0.0014(5) | < 0.001 | 1.72 |
| O | 4 | 1.996(4) | 0.0025(2) | < 0.001 | 1.93 |
| O | 1 | 2.53(2) | 0.0025(2)[d] | 0.016 | 2.33 |
| W | 2 | 3.43(2) | 0.003(1) | 0.011 | 3.38 |
| P | 1 | 3.54(5) | 0.003(1)[d] | 0.018 | 3.52 |
| W | 2 | 3.57(2) | 0.004(2) | < 0.001 | 3.62 |
| O | 6 | 3.97(2) | 0.002(1) | 0.002 | 6 from 3.7 to 4.1 |
| O (MS)[e] | 2 | 4.28(7) | 0.002(1)[d] | 0.034 | 4.05 |
| O | 6 | 4.47(1) | 0.002(1)[d] | < 0.001 | 8 from 4.3 to 4.6 Å |

[a] Fit range: $2 < k < 15$, $1.1 < R < 3.9$, 30 independent data. Fifteen parameters, $S_0^2 = 0.9$, $\Delta E_0 = 71$ eV, $\chi^2 = 25$, $\chi_\nu^2 = 2$, $R = 0.09$. [b] F-test determines the significance of the improvement to the fit created by adding an additional set of atoms. If the $p$ value is less than 0.05, the additional atoms have significantly improved the fit and can be considered "observed" in the EXAFS experiment. [c] Dawson, B. *Acta Crystallogr.* **1953**, *6*, 113−126. [d] Debye−Waller of this shell constrained to be equal to that of the preceding shell. [e] Multiple scattering from the mutually *trans* oxygen ligands

**Table 4.** Best Fit Parameters for the EXAFS Spectrum for $Tc^{V}O$-α1[a]

| neighbor | # of neighbors[b] | distance (Å) | $\sigma^2$ (Å$^2$) | $p(F)$[b] | local structure of the "belt" tungsten site[c] |
|---|---|---|---|---|---|
| O | 1 | 1.640(3) | 0.0013(4) | < 0.001 | 1.72 |
| O | 5 | 1.974(2) | 0.0033(2) | < 0.001 | 2.01 |
| W | 1 | 3.087(4) | 0.0022(5) | 0.014 | 3.37 |
| P | 1 | 3.394(5) | 0.0022(15)[d] | 0.042 | 3.51 |
| O | 5 | 3.31(4) | 0.02(1) | 0.054 | 8 from 3.5 to 4.1 |
| W | 3 | 3.456(7) | 0.0068(7) | < 0.001 | 3.72 |
| O (multiple scatter)[e] | 6 | 4.08(2) | 0.004(3) | 0.001 | 4.05 |
| O | 4 | 4.44(2) | 0.005(2)$^2$ | 0.032 | 5 from 4.4 to 4.5 Å |

[a] Fit range: $2 < k < 14$, $1 < R < 5$; 33 independent data. Sixteen parameters, $S_0^2 = 0.9$, $\Delta E_0 = 4.2(9)$ eV, $\chi^2 = 428$, $\chi_\nu^2 = 26$, $R = 0.009$. [b] F-test determines the significance of the improvement to the fit created by adding an additional set of atoms. If the $p$ value is less than 0.05, the additional atoms have significantly improved the fit and can be considered "observed" in the EXAFS experiment. [c] Dawson, B. *Acta Crystallogr.* **1953**, *6*, 113−126. [d] Debye−Waller of this shell constrained to be equal to that of the preceding single-scattering shell. [e] Multiple scattering due to mutually *trans* oxygen ligands.

shells with a square pyramidal model did not fit the data accurately; an acceptable fit could only be obtained with the typical short Tc(V) bond plus five next-nearest oxygen neighbors. The oxygen neighbors suggested that the Tc was in a pseudo-octahedral rather than square pyramidal geometry. Therefore, the initial Tc model was replaced by one with the TcO unit translated by 0.3 Å toward the phosphate oxygen in the center of the Wells−Dawson ion.

The revised model is in good agreement with the EXAFS data. $Tc^{V}O$-α1 still possesses the short Tc−O bond, 1.64 Å, typical of Tc(V) but has five next-nearest oxygen neighbors at 1.97 Å, rather than the four next-nearest oxygen neighbors found in $Tc^{V}O$-α2. The distance to the nearest W atom is only 3.09 Å, which is much shorter than the nearest distance between neighboring W atoms in the belt of the Wells−Dawson ion, 3.37 Å. Likewise, the distances to the phosphorus at the next nearest W atoms are shorter than expected. Overall, the data suggest that the Tc(V) center in $Tc^{V}O$-α1 has been "pulled into" the Wells−Dawson ion relative to the position of the belt W atom.

A potential explanation for this unexpected structure is suggested by the peak at 37.21 ppm in the $^{183}W$ NMR spectrum of $Tc^{V}O$-α1. A strong positive shift in the $^{183}W$ NMR resonances is associated with two scenarios: two-electron reduced diamagnetic polyoxometalates where the electrons are "delocalized" on the NMR or EPR time scales have been reported for the 2e-reduced α-$[P_2W_{18}O_{62}]^{6-}$, $[W_{10}O_{32}]^{6-}$, and [γ-$SiW_{12}O_{40}]^{6-}$ species.[60−63] Strong positive shifts are also characteristic of the presence of a metal−metal bonding association. The latter was found for the case of [γ-$SiW_{12}S_2O_{38}]^{6-}$ where the deshielded peaks at +1041 ppm correspond to $W^{V}$ atoms of the $\{W_2O_2S_2\}$ fragment.[64] The distances between these $W^{V}$ atoms are quite short (2.815 (1) Å), characteristic of a metal−metal bond involving both the $W^{V}$ centers.

In the $Tc^{V}O$-α1 case, a similar metal−metal bonding may be occurring: the bonding association would involve a dative bond from the occupied Tc $d_{xy}$ orbital into the unoccupied $d_{xy}$ orbital of the W atom at 3.09 Å with which the Tc shares an edge. The presence of the Tc−W interaction also explains why the Tc in $Tc^{V}O$-α1 is less electron rich than the Tc in $Tc^{V}O$-α2, as suggested by the XANES spectrum. The presence of a similar peak in the $^{183}W$ NMR spectrum of $Re^{V}O$-α1 suggests that this complex possesses a similar metal−metal interaction.

**Electrochemistry.** As reported by Nadjo and coworkers,[18] cyclic voltametry (CV) is a sensitive technique used to identify the α1 and α2 isomers and their complexes with transition metals and to assess their purity. In this study, CV has been conducted in aqueous 0.1 M Na-$COOCH_3$ buffer solutions containing 0.5 M $NaSO_4$ at pH 5. The stability of both transition metal-substituted α1/α2 complexes and α1/α2 ligands with this combination of supporting electrolyte and pH has been previously demonstrated.[16,18,58]

Figures 5 and 6 compare the CVs of α2 and α1 lacunary POMs (solid lines) and their respective $Tc^{V}O$ complexes (dotted lines). In each case, the scans are restricted to a region where no derivitization of the electrode surface is observed; proceeding to more negative potentials can lead to the adsorption of reduced species to the electrode surface. The CVs of $Tc^{V}O$-α2 and $Tc^{V}O$-α1 complexes (Figures 5 and 6, respectively) show new waves that are not observed in the lacunary parents. These waves can be attributed to $Tc^{3+}/Tc^{4+}$, $Tc^{4+}/Tc^{5+}$, and $Tc^{5+}/Tc^{6+}$ redox couples within the substituted complex. This is analogous to complexes of the α2 and α1 isomer containing $Cu^{3+}$ or $Fe^{3+}$, where the reduction of the copper or iron occurs before the reduction of the tungsten centers.[57,65] The observed rest potentials for the samples, and the observation of sharply resolved signals in the $^{31}P$ NMR (suggestive of diamagnetic species) allow us to assign the waves ca. −33 and −175 mV (vs Ag/AgCl) as $Tc^{4+}/Tc^{5+}$ redox couples within the α1 and α2 complexes, respectively. Comparison with the $Fe^{2+}/Fe^{3+}$ wave in the compound Fe-α1 reveals that this first step consumes one electron per molecule (see Figure S6, Supporting Information). Waves occurring at more negative potentials are attributed to the reduction of the tungsten framework.

The redox waves occurring at more positive potential are assigned as $Tc^{5+}/Tc^{6+}$ redox couples within the substituted complexes (+990 mV for $Tc^{V}O$-α1 and +813 mV for $Tc^{V}O$-α2). Extending the electrochemical window to more positive potentials allows us to observe a quasi-reversible wave in both compounds. This is assigned to the $Tc^{6+}/Tc^{7+}$ redox process; however, the Tc(VII) species is unstable. Prolonged exposure to positive potentials

(59) Dawson, B. *Acta Crystallogr.* **1953**, 6.
(60) Kazansky, L. P.; Yamase, T. *J. Phys. Chem. A* **2004**, *180*, 6437.
(61) Tézé, A.; Canny, J.; Gurban, L.; Thouvenot, R.; Hervé, G. *Inorg. Chem.* **1996**, *35*, 1001.
(62) Duncan, D. C.; Hill, C. L. *Inorg. Chem.* **1996**, *35*, 5828.
(63) Kozik, M.; Hammer, C. F.; Baker, L. C. W. *J. Am. Chem. Soc.* **1986**, *108*, 2748.
(64) Tézé, A.; Cadot, E.; Béreau, V.; Hervé, G. *Inorg. Chem.* **2001**, *40*, 2000.
(65) Keita, B.; Belhouari, A.; Nadjo, L.; Contant, R. *J. Electroanal. Chem.* **1998**, *442*, 49.

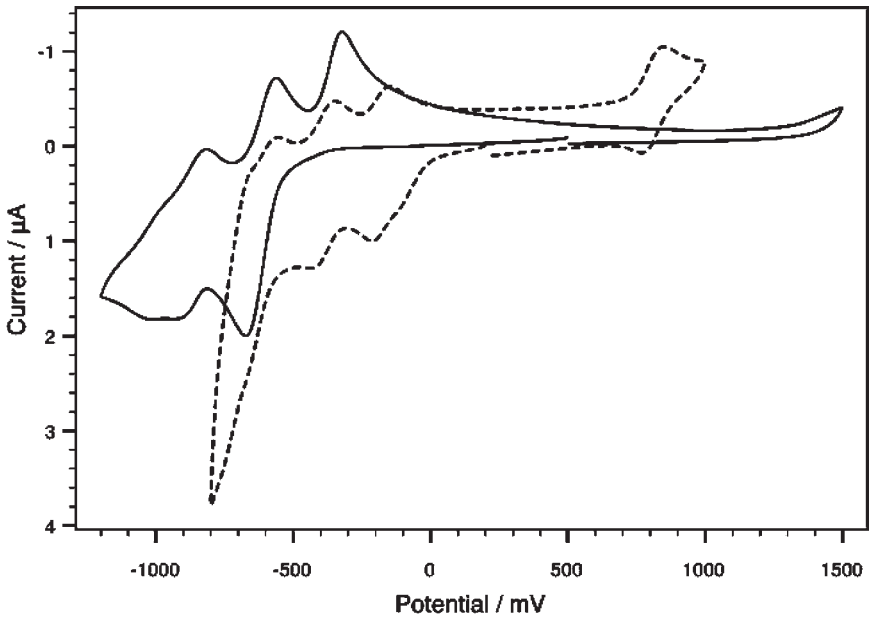


**Figure 5.** Cyclic voltammograms of α2 (solid line) and $Tc^{V}O$-α2 (dashed line) in 0.1 M $CH_3COONa/CH_3COOH$ containing 0.5 M $NaSO_4$, pH = 5.00. Working electrode, glassy carbon; auxiliary electrode, platinum wire; reference electrode, Ag/AgCl. Scan rate = 10 mV $s^{-1}$.

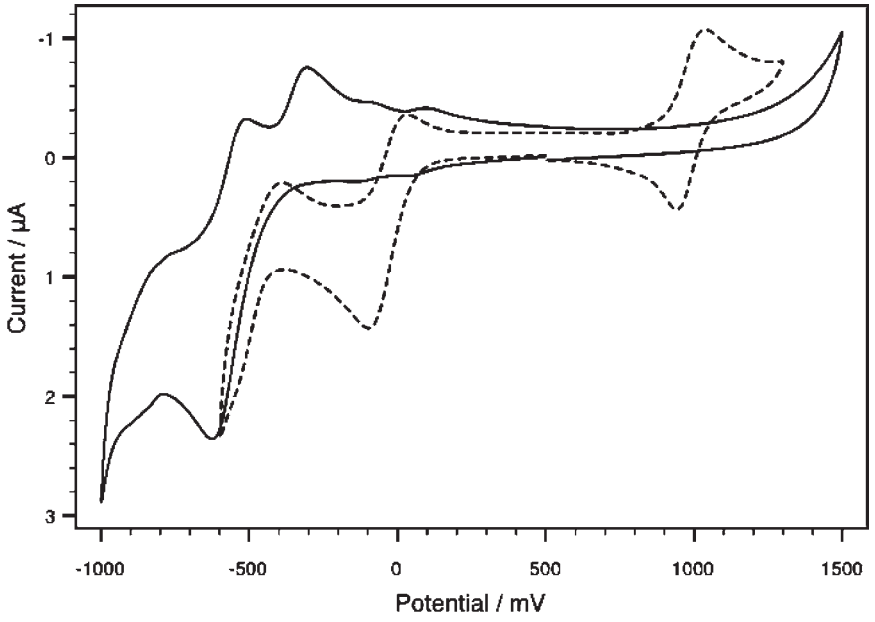


**Figure 6.** Cyclic voltammograms of α1 (solid line) and $Tc^{V}O$-α1 (dashed line) in 0.1 M $CH_3COONa/CH_3COOH$ containing 0.5 M $NaSO_4$, pH = 5.00. Working electrode, glassy carbon; auxiliary electrode, platinum wire; reference electrode, Ag/AgCl. Scan rate = 10 mV $s^{-1}$.

**Table 5.** Halfwave Potentials for the Electroactive $Tc^{V}O$ and $Re^{V}O$ Substituted within the α1 and α2 Frameworks at pH 5, Scan Rate 10 mV $s^{-1}$

| compound | $M^{6+/7+}$ (mV) | $M^{5+/6+}$ (mV) | $M^{4+/5+}$ (mV) |
|---|---|---|---|
| $Tc^{V}O$-α1 | n/a | 990 | −33 |
| $Tc^{V}O$-α2 | n/a | 813 | −175 |
| $Re^{V}O$-α1 | 811.5 | 477.5 | −295 |
| $Re^{V}O$-α2 | 630 | 254 | −284 |

causes dissociation of the complex into a combination of plenary $(P_2W_{18}O_{62})^{6-}$ and lacunary $(P_2W_{17}O_{61})^{10-}$ Wells−Dawson anions and $TcO_4^-$ (as monitored by $^{31}P$ and $^{99}Tc$ NMR). A summary of the observed half-wave potentials is presented in Table 5. In comparison with $Tc^{V}O$-α1, the $Tc^{V}O$-α2 complex exhibits an extra wave at a more negative potential (−386 mV), which we are attributing to a $Tc^{3+}/Tc^{4+}$ redox couple.

A comparison of the $Tc^{4+}/Tc^{5+}$ and $Tc^{5+}/Tc^{6+}$ redox couples in the $Tc^{V}O$-α1 and $Tc^{V}O$-α2 complexes is presented in Figure 7 and summarized in Table 6. The Tc within $Tc^{V}O$-α1 is reduced at more positive potentials than the Tc within $Tc^{V}O$-α2. This is consistent with the trend observed for complexes incorporating first row transition metals.[14,16,18,23] The Tc center located in the belt region of the POM (α1) undergoes more facile reduction than when located in the cap region (α2). This is observed as a difference of 177 mV for the $Tc^{5+}/Tc^{6+}$ redox process and 142 mV for the $Tc^{4+}/Tc^{5+}$ redox process. The more facile reduction of $Tc^{V}O$-α1 relative

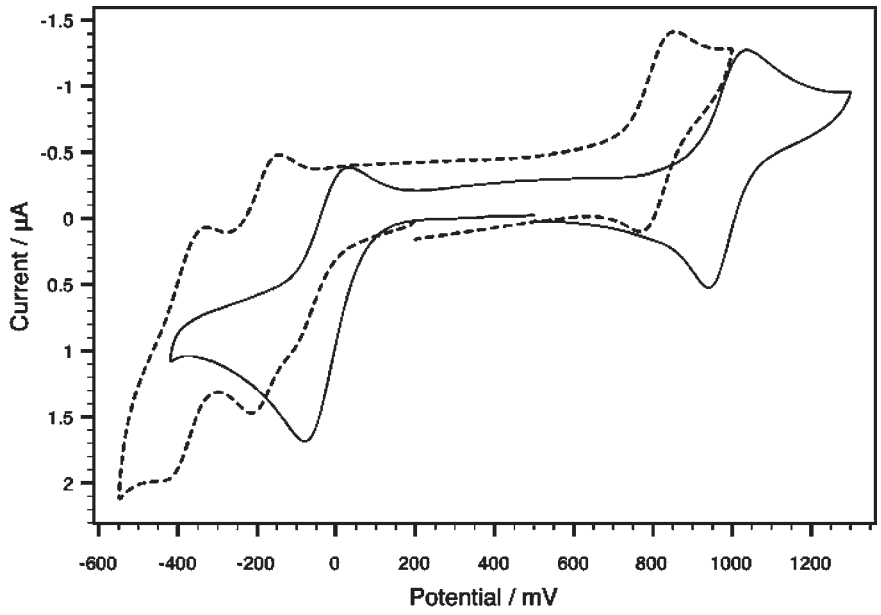


**Figure 7.** Cyclic voltammograms of $Tc^{V}O$-α1 (solid line) and $Tc^{V}O$-α2 (dashed line) in 0.1 M $CH_3COONa/CH_3COOH$, containing 0.5 M $NaSO_4$, pH = 5.00. Working electrode, glassy carbon; auxiliary electrode, platinum wire; reference electrode, Ag/AgCl. Scan rate = 10 mV $s^{-1}$.

**Table 6.** Summary of the Differences in the Half-Wave Potentials between $Tc^{V}O$-α1/$Tc^{V}O$-α2 and $Re^{V}O$-α1/$Re^{V}O$-α2 Complexes and the Differences between the Tc and Re Complexes

| compound | $M^{6+/7+}$ (mV) | $M^{5+/6+}$ (mV) | $M^{4+/5+}$ (mV) |
|---|---|---|---|
| $Tc^{V}O$-α1−$Tc^{V}O$-α2 | n/a | 177 | 142 |
| $Re^{V}O$-α1−$Re^{V}O$-α2 | 181.5 | 223.5 | −11 |
| $Tc^{V}O$-α1−$Re^{V}O$-α1 | n/a | 512.5 | 262 |
| $Tc^{V}O$-α2−$Re^{V}O$-α2 | n/a | 559 | 109 |

to $Tc^{V}O$-α2 may be due the to the Tc−W interaction in $Tc^{V}O$-α1, which should stabilize the lower Tc oxidation states. This highlights the inequivalency of the two sites, and their impact on the chemical properties of transition metal cations substituted in these positions; in this case specifically, the electron transfer properties are unmistakably different.

Figure 8 presents a comparison of the CV traces of the Re-substituted α1 and α2 complexes, and a summary of the half wave potentials is presented in Table 5. A direct assessment of the Re analogues under the same conditions as those of the Tc analyses allows us to correlate the relationships between the substitution position and redox behavior of the metal centers. As with the Tc analogues, new waves at more positive potentials than those of the redox waves of the tungsten framework of the lacunary α1 and α2 are observed. On the basis of the observed rest potentials and the observation of sharp, resolute lines in the $^{31}P$ NMR spectra (indicative of diamagnetic species), we can assign the waves centered at −445 and −443 mV as $Re^{3+}/Re^{4+}$ redox couples, those at −295 and −284 mV as $Re^{4+}/Re^{5+}$ redox couples, the waves at +477 and +254 mV as $Re^{5+}/Re^{6+}$ redox processes, and the waves at +822 and +627 mV as $Re^{6+}/Re^{7+}$ redox couples (for $Re^{V}O$-α1 and $Re^{V}O$-α2, respectively). The assignment of the quasi-reversible waves at +822 and +627 mV as $Re^{6+}/Re^{7+}$ is analogous to those in the Tc complexes.

Prolonged exposure to oxidative potentials (greater that +870 mV) causes the complexes to dissociate irreversibly into a combination of plenary $(P_2W_{18}O_{62})^{6-}$ and lacunary $(P_2W_{17}O_{61})^{10-}$ Wells−Dawson anions and $ReO_4^-$ (as judged by $^{31}P$ NMR and electrochemistry). A comparison of the various waves is presented in Table 6. The redox processes in the belt region consistently occur at potentials about 200 mV more positive than those of the cap region. This is parallel to what is observed in the Tc examples, albeit the reduction/oxidation of the Re is decidedly more impacted by the substitution, i.e, the average $E_{1/2}(Re^{V}O$-α1) − $E_{1/2}(Re^{V}O$-α2) = 202 mV and the average $E_{1/2}$-($Tc^{V}O$-α1) − $E_{1/2}$ ($Tc^{V}O$-α2) = 160 mV.

Upon comparison of the redox couples for $Re^{V}O$-α1 and $Re^{V}O$-α2 (Table 6), a difference of 223.5 and 181.5 mV is observed for the $Re^{5+}/Re^{6+}$ and the $Re^{6+}/Re^{7+}$ waves, respectively. As with the Tc complexes, this trend is consistent with stabilization of the lower oxidation states in $Re^{V}O$-α1 by formation of a Re−W interaction. This trend is not apparent for what are assigned as $Re^{3+}/Re^{4+}$ and $Re^{4+}/Re^{5+}$ couples. The difference in the position of the redox waves differs by ca. −11 mV (vs Ag/AgCl), which indicates that either (i) these waves are actually due to redox processes involving the tungsten framework and the $Re^{3+}/Re^{4+}$ and $Re^{4+}/Re^{5+}$ couples are eclipsed or (ii) the $Re^{3+}/Re^{4+}$ and $Re^{4+}/Re^{5+}$ couples are unaffected by substitution position. This is currently undergoing investigation using *in situ* spectroelectrochemistry.

Figure 9 presents a comparison of the CVs of the family of α2 and α1 complexes. Figure 9A shows the voltammograms of $Tc^{V}O$-α2 (dotted line) and $Re^{V}O$-α2 (solid line); Figure 9B shows the voltammograms of $Tc^{V}O$-α1 (dotted line) and $Re^{V}O$-α1 (solid line). It can be seen that the reduction of Tc(VI) to Tc(V) is more facile than that of Re(VI) to Re(V) by 559 mV (Table 6) within the cap-substituted α2 complexes. This trend is paralleled in the α1 complexes, but the difference between the M(VI) to M(V) reduction is 512 mV. When comparing the differences in potential for the reduction of M(V) to M(IV), the more favorable process again lies with the Tc complexes, but the ease with which this occurs compared to the Re congener is

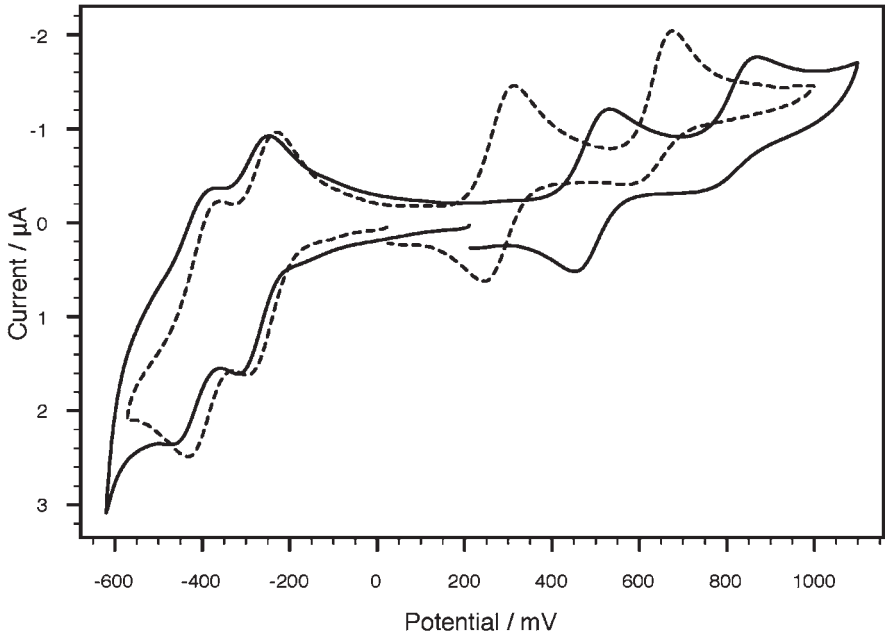


**Figure 8.** Cyclic voltammograms of $Re^{V}O$-α1 (solid line) and $Re^{V}O$-α2 (dotted line) in 0.1 M $CH_3COONa/CH_3COOH$ containing 0.5 M $NaSO_4$, pH = 5.00. Working electrode, glassy carbon; auxiliary electrode, platinum wire; reference electrode, Ag/AgCl. Scan rate = 10 mV $s^{-1}$.

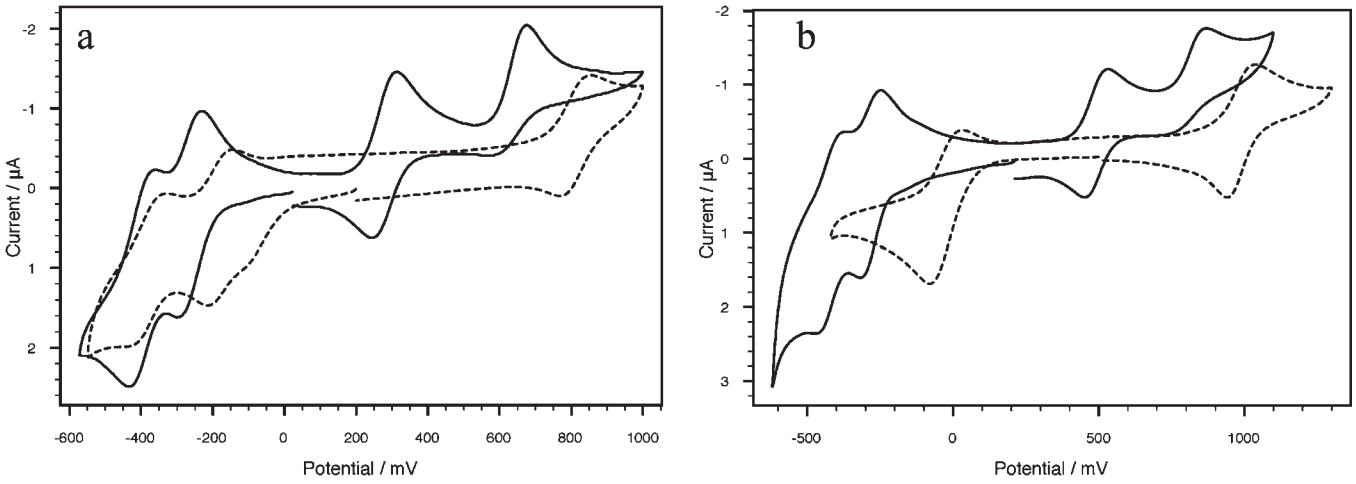


**Figure 9.** Cyclic votammograms of Tc and Re complexes. (A) $Re^{V}O$-α2 (solid line) and $Tc^{V}O$-α2 (dotted line). (B) $Re^{V}O$-α1 (solid line) and $Tc^{V}O$-α1 (dotted line) in 0.1 M $CH_3COONa/CH_3COOH$ containing 0.5 M $NaSO_4$, pH = 5.00. Working electrode, glassy carbon; auxiliary electrode, platinum wire; reference electrode, Ag/AgCl. Scan rate = 10 mV $s^{-1}$.

different between the α2 (109 mV) and the α1 (262 mV) complexes.

All of the electrochemical studies, described above, along with multinuclear NMR and mass spectrometry clearly confirm that the technetium center present within the structure of the compounds $Tc^{V}O$-α1 and $Tc^{V}O$-α2 is in the +V oxidation state. This Tc(V) center can be reduced to Tc(IV) or oxidized to Tc(VI). Other oxidation states (+III and +VII) have been identified in other electrolytes, and these studies will be published elsewhere.

## Conclusion

Understanding and controlling the extensive redox chemistry of $^{99}Tc$ is one of the obstacles in identifying separation strategies, and the identification and development of appropriate waste forms for containing $^{99}Tc$ once separated from nuclear fuel and waste tanks. We are approaching this problem from a molecular-level vantage point by employing polyoxometalates to address the coordination chemistry and redox stability of Tc within metal oxide matrices.

In this study, we report the synthesis and physical chemical properties of $Tc^{V}O$ incorporated into the lacunary α1 and α2 polyoxometalates. These syntheses rely on the use of a "transfer ligand", ethylene glycol, which facilitates the stabilization of the $Tc^{V}O$ core as the complexes are formed. The complexes were characterized by multinuclear NMR spectroscopy, X-ray spectroscopy, and electrochemistry. Together, these techniques provide compelling evidence that the Tc(V) is incorporated in the α1 and α2 frameworks.

Transition metal cations substituted into the α1 and α2 positions clearly show differences in electrochemistry; specifically, transition metal cations substituted into the α1 position are more readily reduced than when substituted into the α2 position.[14,16,18,23] These differences may be explained by the differences in the local structures of Tc in these complexes

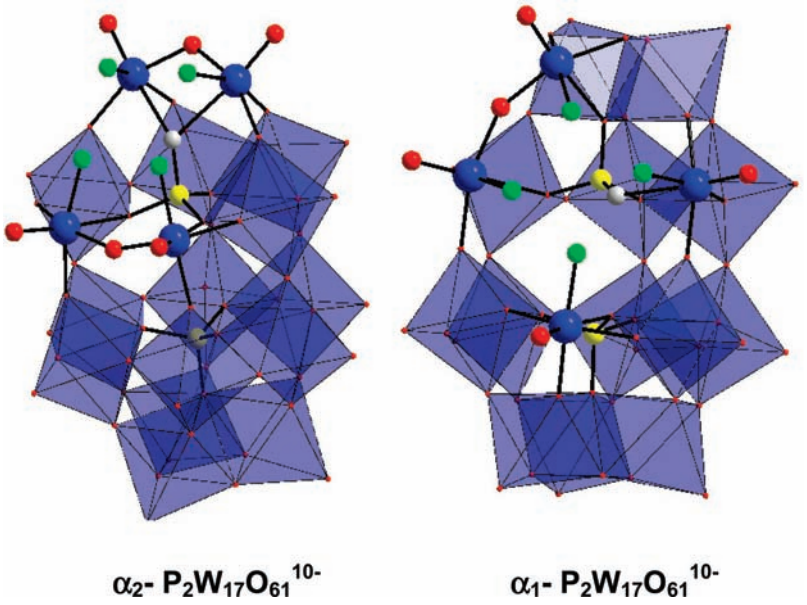


**Figure 10.** Representations of the defect sites of α2 and α1. The tungsten atoms that create the defect are shown as balls. The tungsten atoms not closely associated with the defect site are represented as octahedra. The oxygen atoms bound to the W atoms of the defect are shown in green. All other oxygen atoms bound to W atoms are shown in red. The P atoms are yellow. The oxygen atom bound to the phosphorus of the defect is shown in off-white. In the α2 site, this oxygen atom is bound to two W atoms and the P atom; in the α1 site, this oxygen atom is bound to one W atom and the P atom.

as determined by EXAFS. The ease of reduction for metal ions coordinated in the $\alpha_1$ position is consistent with the formation of a dative metal−metal bond between Tc(V) and the nearest tungsten atom in the lacunary Wells−Dawson ion. The defects of α1 and α2 are shown in Figure 10. The basic oxygen of the α1 defect (gray in Figure 10) is bound to the phosphorus atom and one tungsten atom; in contrast, the corresponding oxygen of the α2 defect is bound to the one phosphorus atom and two tungsten atoms. The oxygen of the α1 site would thus favor stronger interaction of the transition metal with the W atoms in the belt. Theoretical treatments are consistent with these findings; the LUMO in the frontier orbitals of the parent $(\alpha\text{-}P_2W_{18}O_{61})^{6-}$ $(a''_1)$ consists of 96% α1 character.[66]

This reduction behavior is illustrated in this study wherein $Tc^VO$ is substituted into the α1 and α2 defects. The reduction of Tc(V) to Tc(IV) indeed is facilitated in the $Tc^VO$-α1 isomer compared to the $Tc^VO$-α2 isomer (+157 mV). To evaluate and quantify the influence due to the specific isomers, we must operate under conditions where the influence of protonation is negligible, i.e., at pH equal to or greater than 7. A full electrochemical study as a function of pH and comparison with DFT calculations to compare the energies of $Tc^VO$-α1 and $Tc^VO$-α2 will be forthcoming.

**Acknowledgment.** Part of this work was performed at Lawrence Berkeley National Laboratory and was supported by the Director, Office of Science, Office of Basic Energy Sciences of the U.S. Department of Energy (DOE) under Contract No. DE-AC02-05CH11231. Portions of this research were carried out at the Stanford Synchrotron Radiation Laboratory, a national user facility operated by Stanford University on behalf of the U.S. DOE, Office of Basic Energy Sciences. Use of the Advanced Photon Source at Argonne was supported by the U.S. Department of Energy, Office of Science, Office of Basic Energy Sciences, under Contract No. DE-AC02-06CH11357. We are grateful to the NSF (Grant Nos. CHE 0414218 and CHE 0750118) for the research performed at Hunter College. We are also grateful to DE-FG02-09ER16097 (Heavy Element Chemistry, Office of Science, Department of Energy) for support of this work. The research Infrastructure at Hunter College is partially supported by NIH-Research Centers in Minority Institutions Grant RR03037-08.

**Supporting Information Available:** Figures showing the column purification of $Re^VO$-α1 (Figure S1); infrared spectra of $Tc^VO$-α1 and $Tc^VO$-α2 (Figure S2); mass spectra for $Tc^VO$-α1 and $Tc^VO$-α2 (Figure S3); $^{183}W$ NMR for an independent synthesis of $Tc^VO$-α1 (Figure S4); EXAFS data for $Tc^VO$-α2 taken at the Advanced Photon Source, Argonne National Laboratory (Figure S5). Also included are the CVs of $Tc^VO$-α1 and Fe-α1 (Figure S6). Table S1 shows the best fit parameters for $Tc^VO$-α2 taken at the APS at Argonne National Laboratory. This material is available free of charge via the Internet at http://pubs.acs.org.

**Note Added after ASAP Publication.** This paper was published on the Web on January 26, 2011, with the incorrect number of half-life years in the first line of the Abstract. The corrected version was reposted on February 2, 2011.

(66) Lopez, X.; Bo, C.; Poblet, J. M. *J. Am. Chem. Soc.* **2002**, *124*, 12574.